RESEARCH ARTICLE

Figures and figure supplements

An increase of inhibition drives the developmental decorrelation of neural activity

Mattia Chini *et al*

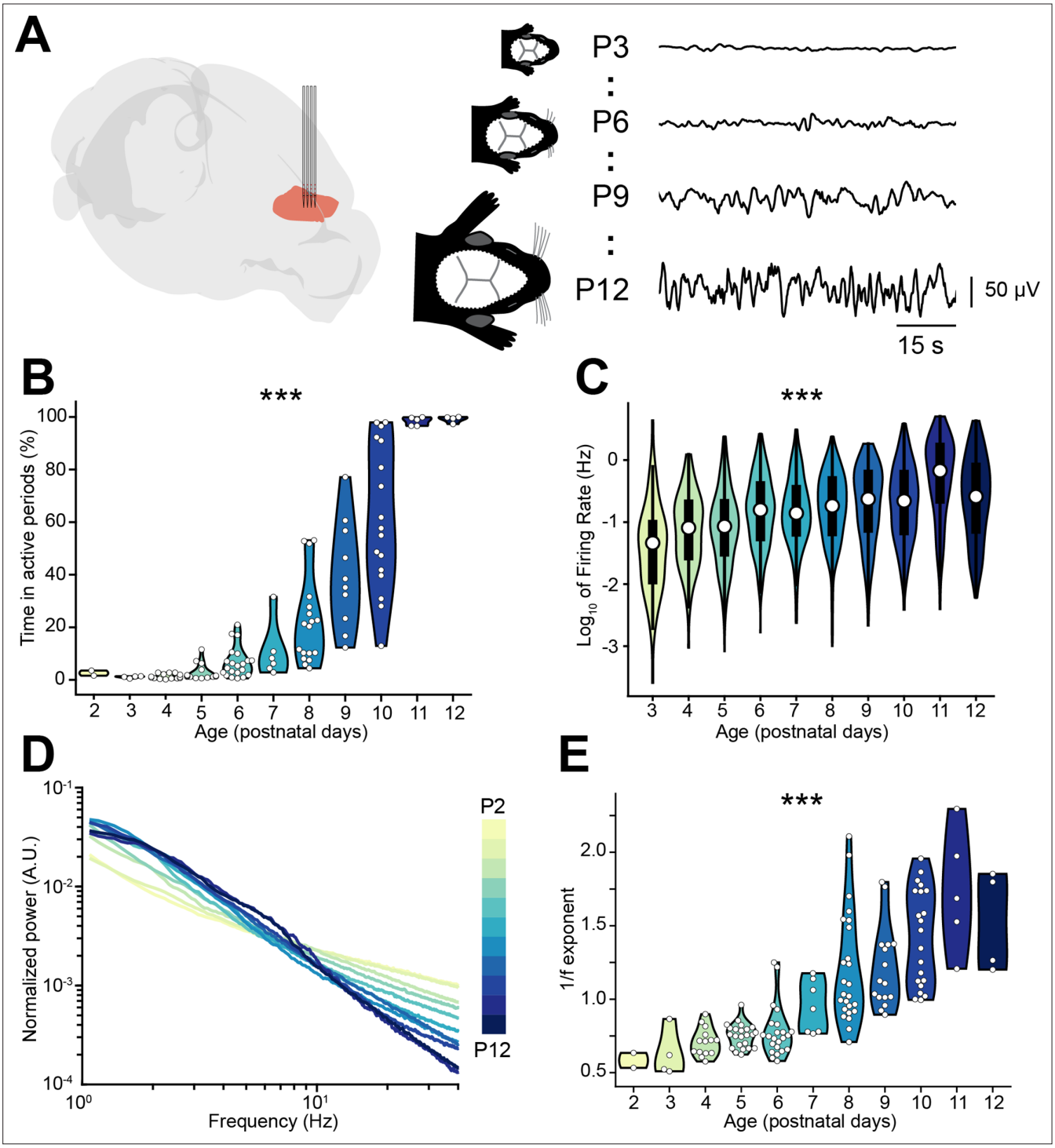

Figure 1. Active periods and local field potential (LFP) properties of the mouse medial prefrontal cortex (mPFC) across the first 2 postnatal weeks. (**A**) Schematic representation (***Claudi et al., 2021***) of extracellular recordings in the mPFC of P2-12 mice (left), and representative LFP traces from P3, P6, P9, and P12 mice (right). (**B and C**) Violin plots displaying the percentage of time spent in active periods (**B**) and the single unit activity (SUA) firing rate (**C**) of P2-12 mice (n=117 mice and 2269 single units, respectively). (**D**) Log-log plot displaying the normalized median power spectral density (PSD) power in the 1–40 Hz frequency range of P2-12 mice (n=117 mice). Color codes for age with 1 day increment. (**E**) Violin plot displaying the 1/f exponent of P2-12 mice (n=117 mice). In (**B**) and (**E**) white dots indicate individual data points. In (**C**) data are presented as median, 25th, 75th percentile, and interquartile range. In (**B**), (**C**), and (**E**) the shaded area represents the probability distribution density of the variable. In (**D**) data are presented as median. Asterisks in (**B**), (**C**), and (**E**) indicate significant effect of age. ***p<0.001. Generalized linear models (**B–C**) and linear model (**E**). For detailed statistical results, see ***Supplementary file 1***.

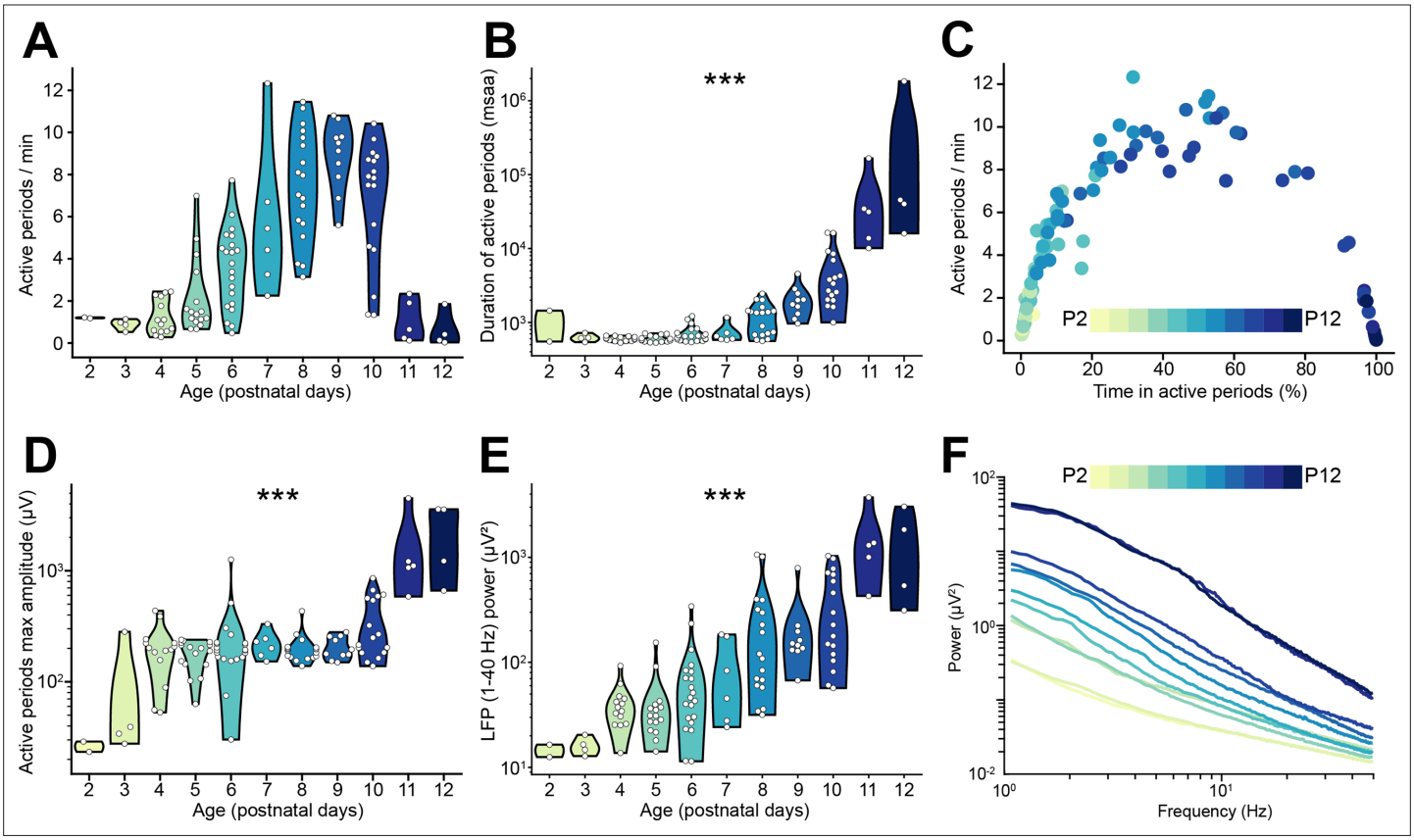

Figure 1—figure supplement 1. Local field potential (LFP) and single unit activity (SUA) properties of the mouse medial prefrontal cortex (mPFC) across the first 2 postnatal weeks. (**A and B**) Violin plots displaying the number (**A**) and duration (**B**) of active periods of P2-12 mice (*n*=117 mice). (**C**) Scatter plot displaying the time spent in active periods with respect to the number of active periods per minute of P2-12 mice (*n*=117 mice). Color codes for age. (**D and E**) Violin plot displaying the maximum amplitude of active periods (**D**) and the LFP power in the 1–40 Hz frequency range (**E**) of P2-12 mice (*n*=117 mice). (**F**) Log-log line plot displaying the median LFP power in the 0.1–4 Hz frequency range of P2-12 mice (*n*=117 mice). Color codes for age. In (**A**), (**B**), (**D**), and (**E**) white dots indicate individual data points and the shaded area represents the probability distribution density of the variable. In (**F**) data are presented as median. Asterisks in (**B**), (**D**), and (**E**) indicate significant effect of age. ***p<0.001. Generalized linear models. For detailed statistical results, see ***Supplementary file 1***.

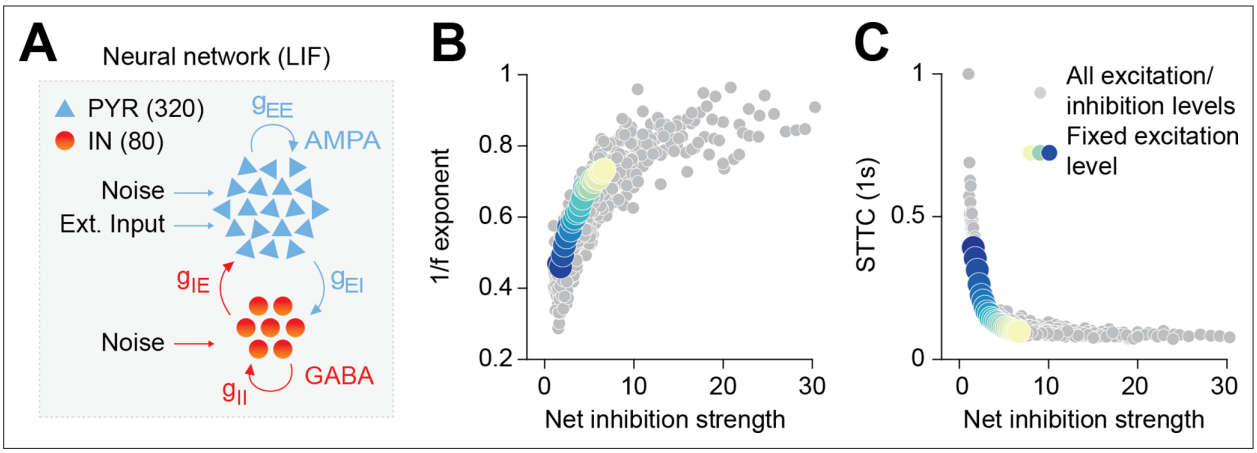

Figure 2. Increased inhibition leads to an increase in the 1/f exponent and decorrelates spike trains in a neural network model. (**A**) Schematic representation of the neural network model. (**B**) Scatter plot displaying the 1/f exponent as a function of net inhibition strength. (**C**) Scatter plot displaying average STTC as a function of net inhibition strength. For (**B**) and (**C**) color codes for inhibition strength with fixed excitation level.

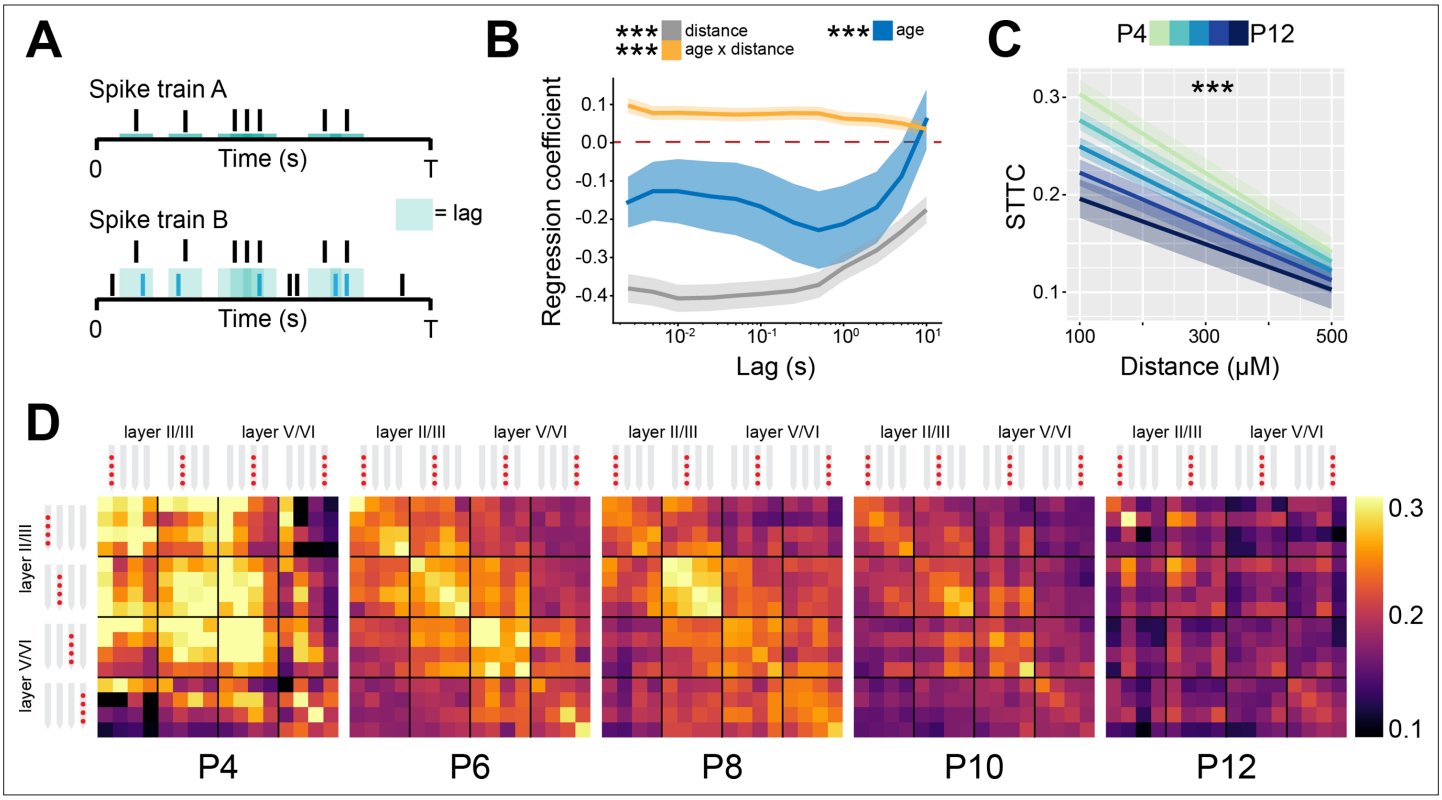

Figure 3. Spike time tiling coefficient (STTC) decreases throughout development with a specific spatial profile in the mouse medial prefrontal cortex (mPFC). (**A**) Schematic representation of the STTC quantification. (**B**) Multivariate linear regression coefficients with respect to STTC lag (*n*=40,921 spike train pairs and 82 mice). (**C**) Average STTC at 1 s lag of P4, P6, P8, P10, and P12 mice over distance (*n*=40,921 spike train pairs and 82 mice). Color codes for age. (**D**) Weighted adjacency matrices displaying average STTC at 1 s lag of P4, P6, P8, P10, and P12 mice as a function of the recording sites in which the spike train pair has been recorded. Color codes for STTC value. In (**B**) regression coefficients are presented as mean and 95% CI. In (**C**) data are presented as mean ± SEM. Asterisks in (**B**) indicate significant regression coefficients of the respective (interaction between) variables for STTC at 1 s lag. Asterisks in (**C**) indicate significant effect of age*distance interaction. ***p<0.001. Linear mixed-effect models. For detailed statistical results, see ***Supplementary file 1***.

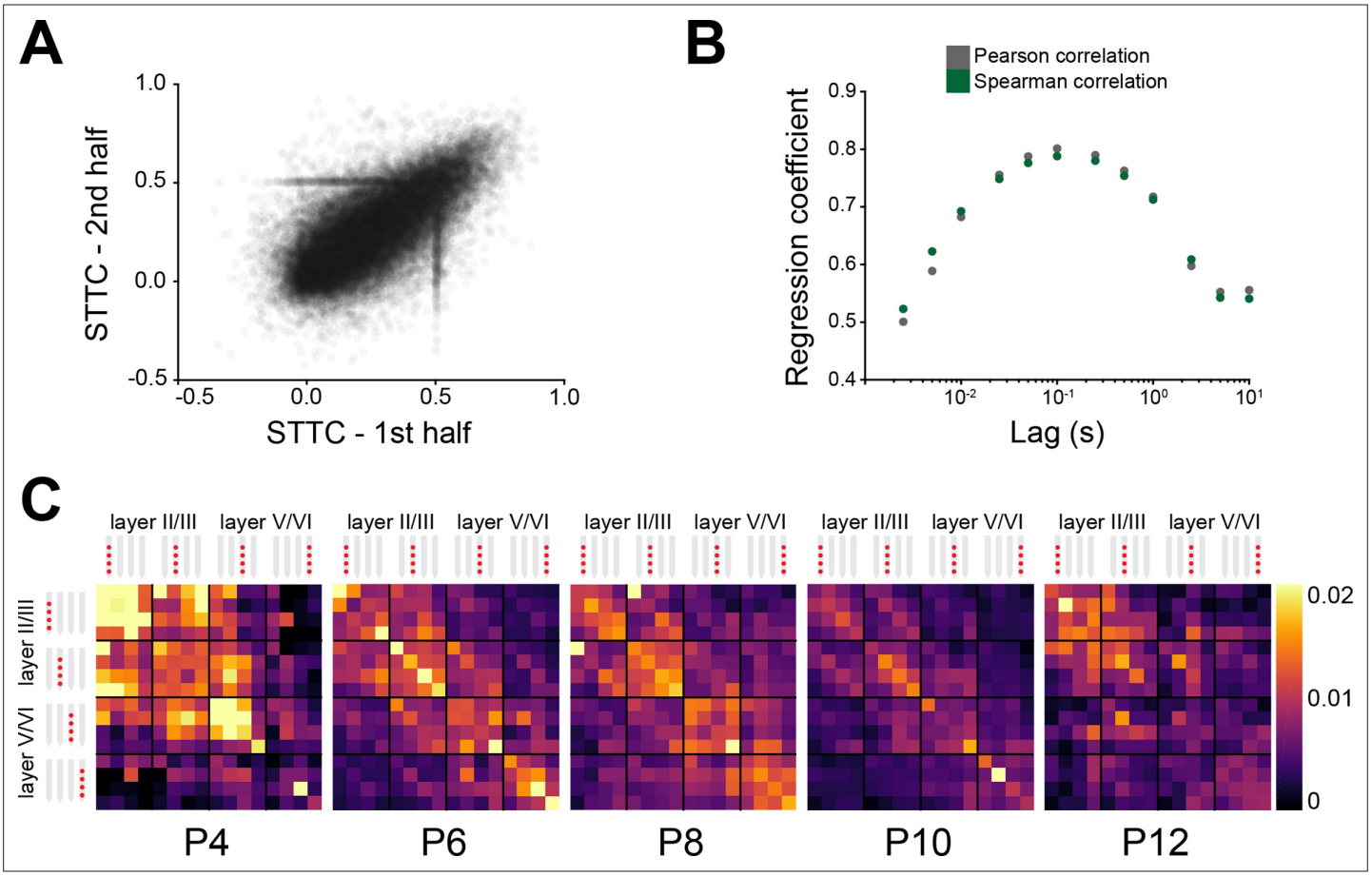

Figure 3—figure supplement 1. The spike time tiling coefficient (STTC) developmental decrease follows specific spatial patterns in the mouse medial prefrontal cortex (mPFC). (**A**) Scatter plot displaying the STTC computed in the first half of the recording with respect to STTC computed in the second half of the recording (*n*=40,921 spike train pairs and 82 mice). (**B**) Scatter plot displaying Pearson and Spearman correlation coefficient for STTC computed on the first and second half of the recording over lags (*n*=40,921 spike train pairs and 82 mice). (**C**) Weighted adjacency matrices displaying average STTC at 2.5 ms lag of P4, P6, P8, P10, and P12 mice as a function of the recording sites in which the spike train pair has been recorded. Color codes for STTC value. For detailed statistical results, see ***Supplementary file 1***.

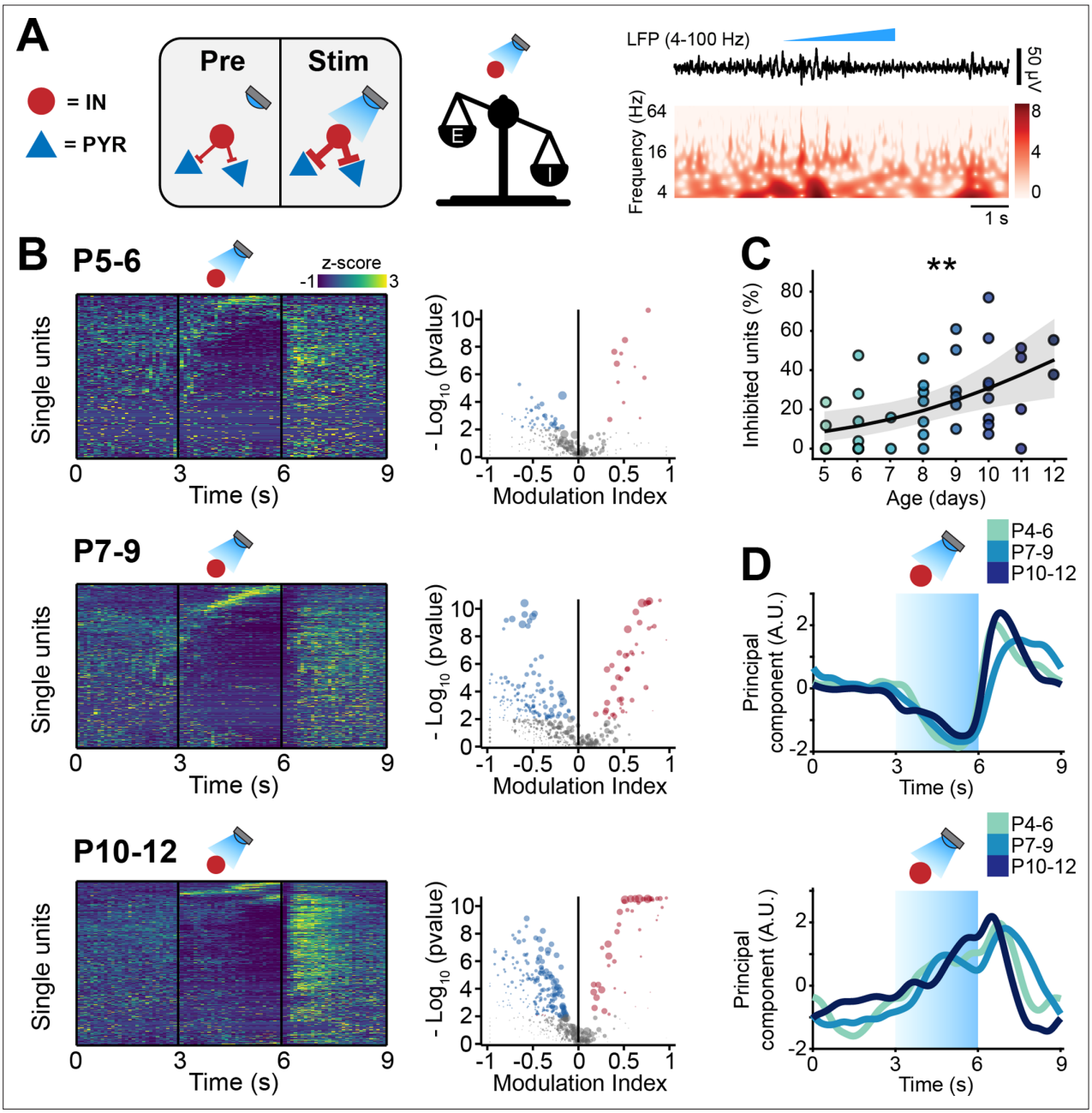

Figure 4. Optogenetic stimulation of interneuron (IN) activity leads to widespread inhibition in the developing mouse medial prefrontal cortex (mPFC). (**A**) Schematic representation of the effects induced by optogenetic IN stimulation (left). Representative local field potential (LFP) trace (4–100 Hz band-pass filter) with a corresponding wavelet spectrum at an identical timescale during ramp light stimulation (473 nm, 3 s) of INs in the mPFC of a P10 mouse. (**B**) Z-scored single unit firing rates in response to optogenetic stimulation of INs (left) and volcano plot displaying the modulation index of pre vs. stim single unit firing rates (right) for P4-6 (top, *n*=268 units and 5 mice), P7-9 (middle, *n*=480 units and 7 mice), and P10-12 (bottom, *n*=475 units and 7 mice) mice. Color codes for firing rate. (**C**) Scatter plot displaying the percentage of inhibited units with respect to age (*n*=19 mice). (**D**) First (top, putative pyramidal neurons [PYRs]) and second (bottom, putative INs) principal component analysis (PCA) component of trial-averaged spike trains in response to optogenetic stimulation of INs. Color codes for age group. In (**C**) the regression is presented as mean and 95% CI. Asterisks in (**C**) indicate significant effect of age. **p<0.01. Individual dots in (**C**) indicate distinct optogenetic protocols (up to two per mouse, for details see Materials and methods). Generalized linear mixed-effect model (**C**). For detailed statistical results, see ***Supplementary file 1***.

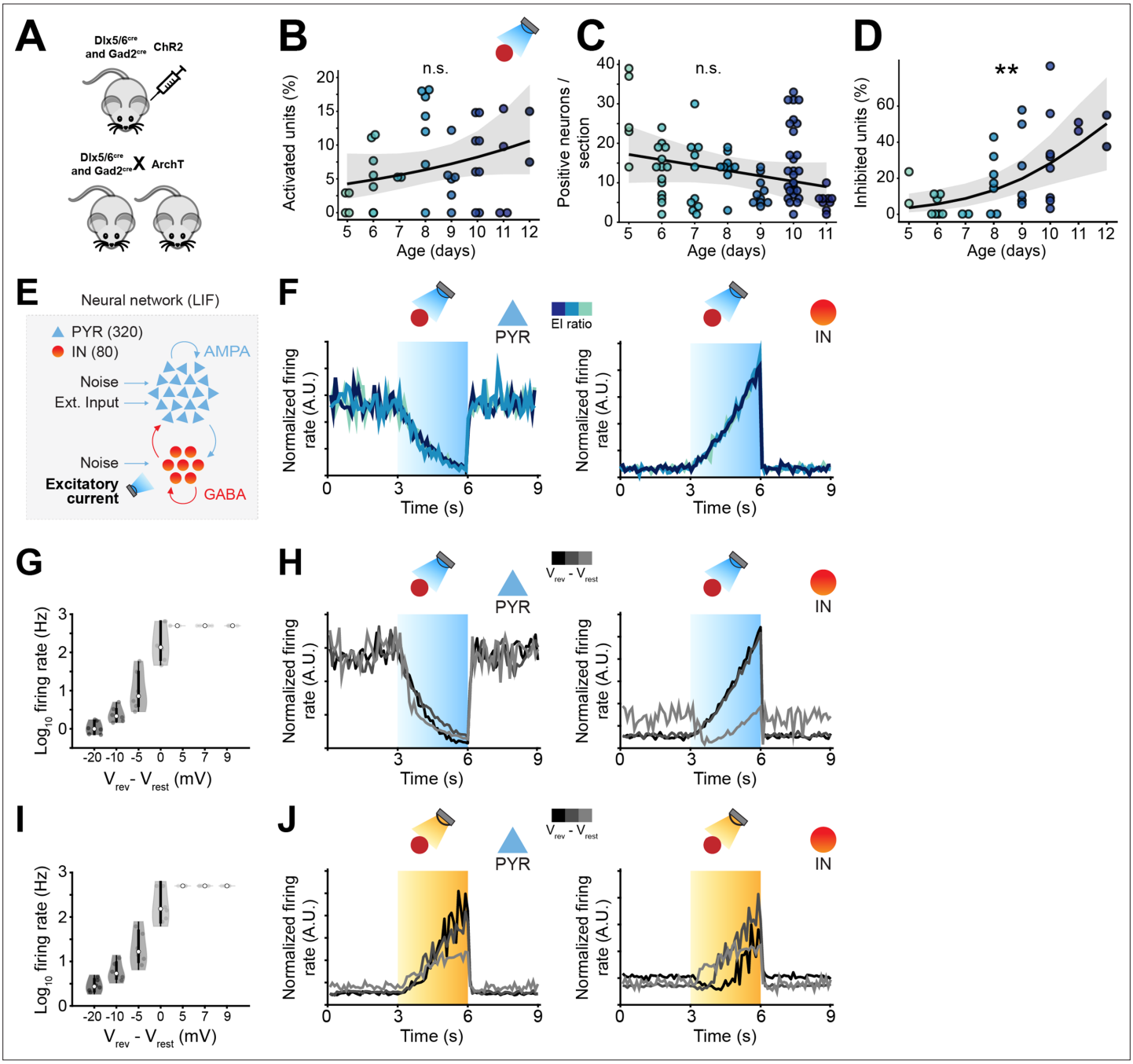

Figure 4—figure supplement 1. Optogenetic manipulation of interneuron (IN) activity affects local field potential (LFP) activity in the mouse developing medial prefrontal cortex (mPFC). (**A**) Schematic representation of the experimental approach employed to target INs with an excitatory and an inhibitory opsin. (**B**) Proportion of activated units in response to ramp light stimulation of INs as a function of age (n=19 mice). (**C**) Number of virally transfected neurons as a function of age (n=87 images and 16 mice). (**D**) Scatter plot displaying the percentage of inhibited units (restricted to the top 50% units for firing rate) with respect to age (n=19 mice). (**E**) Schematic representation of the neural network model. (**F**) Modeled pyramidal neurons (PYRs) (top) and INs (bottom) trial-averaged normalized firing rate in response to optogenetic stimulation of INs. Color codes for excitation-inhibition (E-I) ratio. (**G**) Violin plot displaying the log-transformed firing rate in simulated optogenetic experiments with an excitatory current injected into INs as a function of the difference between the chloride reverse potential and the membrane resting potential. (**H**) Modeled PYRs (top) and INs (bottom) trial-averaged normalized firing rate in response to optogenetic stimulation of INs. Color codes for the difference between the chloride reverse potential and the membrane resting potential. (**I, J**) Same as (**G, H**) for simulated optogenetic experiments with an inhibitory current injected into INs. In (**B–D**) and (**C**) the regression is presented as mean and 95% CI. Asterisks in (**D**) indicate significant effect of age. ***p<0.001. Individual dots in (**B**) and (**D**) indicate distinct optogenetic protocols (up to two per mouse, for details, see Materials and methods). Generalized linear mixed-effect model (**B**) and (**D**), linear mixed-effect model (**C**). For detailed statistical results, see ***Supplementary file 1***.

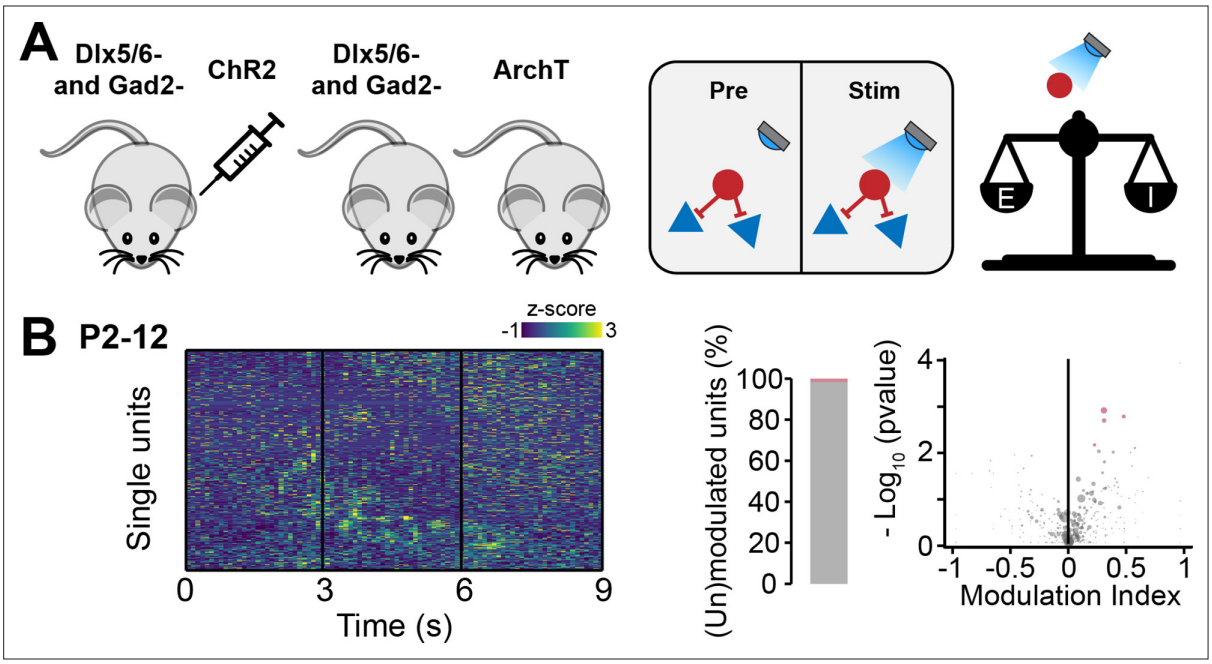

Figure 4—figure supplement 2. Optogenetic manipulation of interneuron (IN) activity in cre- mice does not affect the developing mouse medial prefrontal cortex (mPFC). (**A**) Schematic representation of the experimental approach employed to generate control (cre-) mice (left) and schematic representation of the lack of effects induced by optogenetic IN stimulation in cre- mice (right). (**B**) Z-scored single unit firing rates response to optogenetic stimulation in cre- mice (left) and volcano plot displaying the modulation index of pre vs. stim single unit firing rates (right) for P2-12 mice (*n*=380 units and 10 mice),.

Figure 5. Optogenetic inhibition of interneuron (IN) activity leads to widespread excitation in the developing mouse medial prefrontal cortex (mPFC). (**A**) Schematic representation of the effects induced by optogenetic IN inhibition (left). Representative local field potential (LFP) trace (4–100 Hz band-pass filter) with a corresponding wavelet spectrum at an identical timescale during ramp light stimulation (594 nm, 3 s) of INs in the mPFC of a P10 mouse. (**B**) Z-scored single unit firing rates in response to optogenetic stimulation of INs (left) and volcano plot displaying the modulation index of

Figure 5 continued on next page

Figure 5 continued

pre vs. stim single unit firing rates (right) for P2-3 (top left, *n*=164 units and 5 mice), P4-6 (top right, *n*=286 units and 11 mice), P7-9 (bottom left, *n*=470 units and 13 mice), and P10-12 (bottom right, *n*=691 units and 11 mice) mice. Color codes for firing rate. (**C**) Scatter plot displaying the percentage of activated units with respect to age (*n*=40 mice). (**D**) first (top) and second (bottom) principal component analysis (PCA) component of trial-averaged spike trains in response to optogenetic inhibition of INs. Color codes for age. (**E**) Schematic representation of the neural network model. (**F**) Modeled pyramidal neurons (PYRs) (left) and INs (right) trial-averaged normalized firing rate in response to optogenetic inhibition of INs. Color codes for excitation-inhibition (E-I) ratio. In (**C**) the regression is presented as mean and 95% CI. Asterisks in (**C**) indicate significant effect of age. ***p<0.001. Individual dots in (**C**) indicate distinct optogenetic protocols (up to two per mouse, see Materials and methods). Generalized linear mixed-effect model (**C**). For detailed statistical results, see ***Supplementary file 1***.

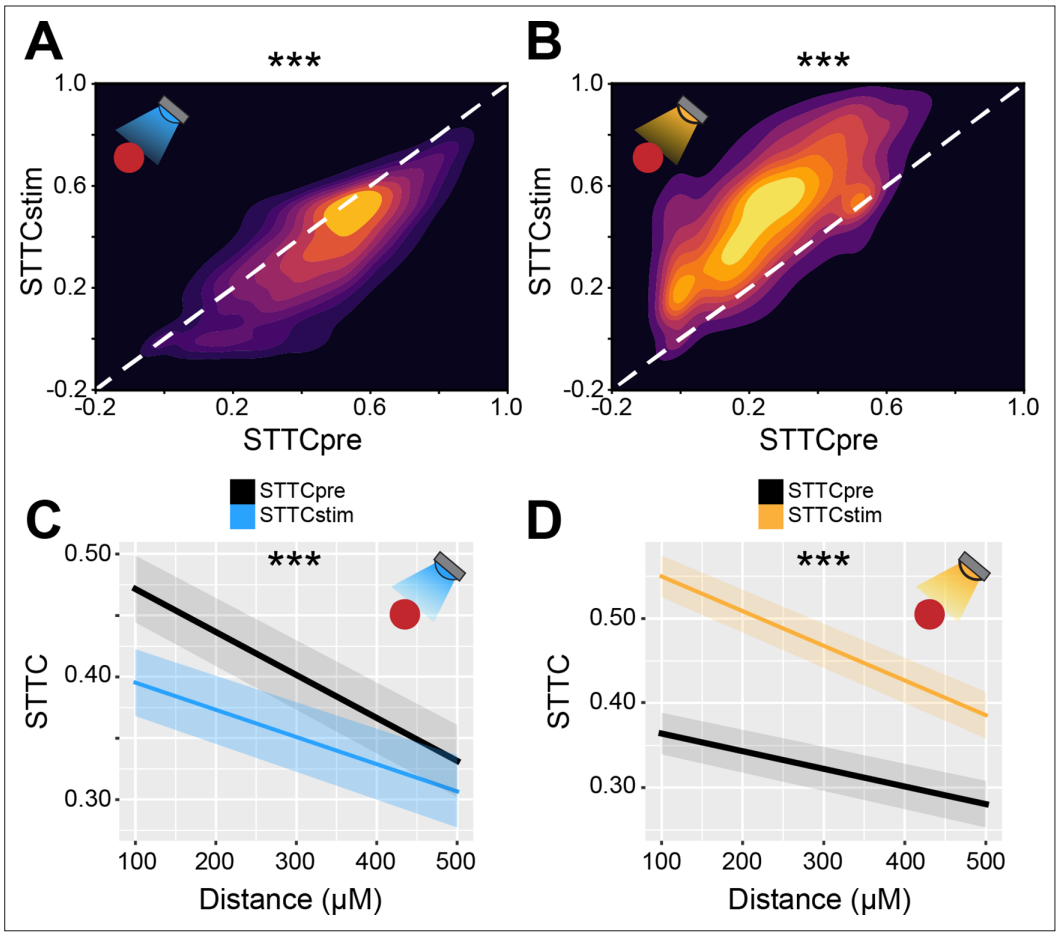

Figure 6. Bidirectional optogenetic manipulation of interneuron (IN) activity affects spike time tiling coefficient (STTC) in the developing mouse medial prefrontal cortex (mPFC). (**A and B**) 2D kernel density plots displaying STTC before IN optogenetic manipulation (STTCpre) and STTC during optogenetic manipulation (STTCstim) during IN activation (**A**) and inhibition (**B**) (n=10,173 spike train pairs and 19 mice, n=9778 spike train pairs and 40 mice, respectively). (**C and D**) Average STTCpre and STTCstim during IN activation (**C**) and inhibition (**D**) over distance (n=10,173 spike train pairs and 19 mice, n=9778 spike train pairs and 40 mice, respectively). In (**C and D**) data are presented as mean ± SEM. Asterisks in (**A and B**) indicate significant effect of IN activation and inhibition, respectively. Asterisks in (**C and D**) indicate significant effect of IN activation*distance and IN inhibition*distance interaction, respectively. ***p<0.001. Linear mixed-effect models. For detailed statistical results, see ***Supplementary file 1***.

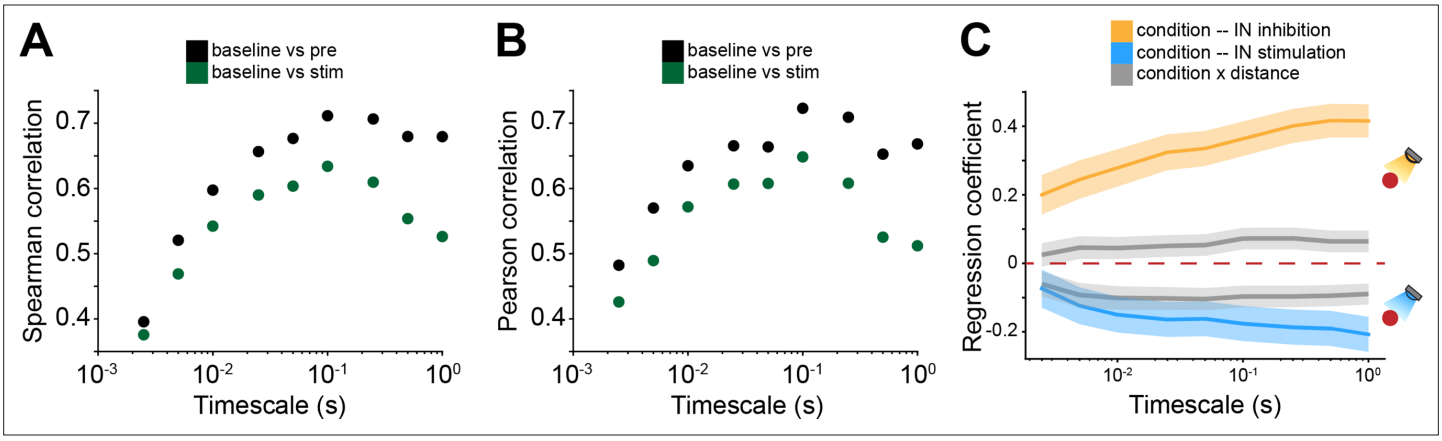

Figure 6—figure supplement 1. Bidirectional optogenetic manipulation of interneuron (IN) activity effects on spike time tiling coefficient (STTC) depends on spatial configurations and age. (**A and B**) Scatter plot displaying Pearson (**A**) and Spearman (**B**) correlation coefficients for STTC before IN optogenetic manipulation (STTCpre) and STTC during optogenetic manipulation (STTCstim) with STTC computed on baseline data over lags (*n*=19,951 spike train pairs and 59 mice). (**C**) Multivariate linear regression coefficients as a function of STTC lag (*n*=19,951 spike train pairs and 59 mice). In (**C**) regression coefficients are presented as mean and 95% CI. Linear mixed-effect models. For detailed statistical results, see ***Supplementary file 1***.

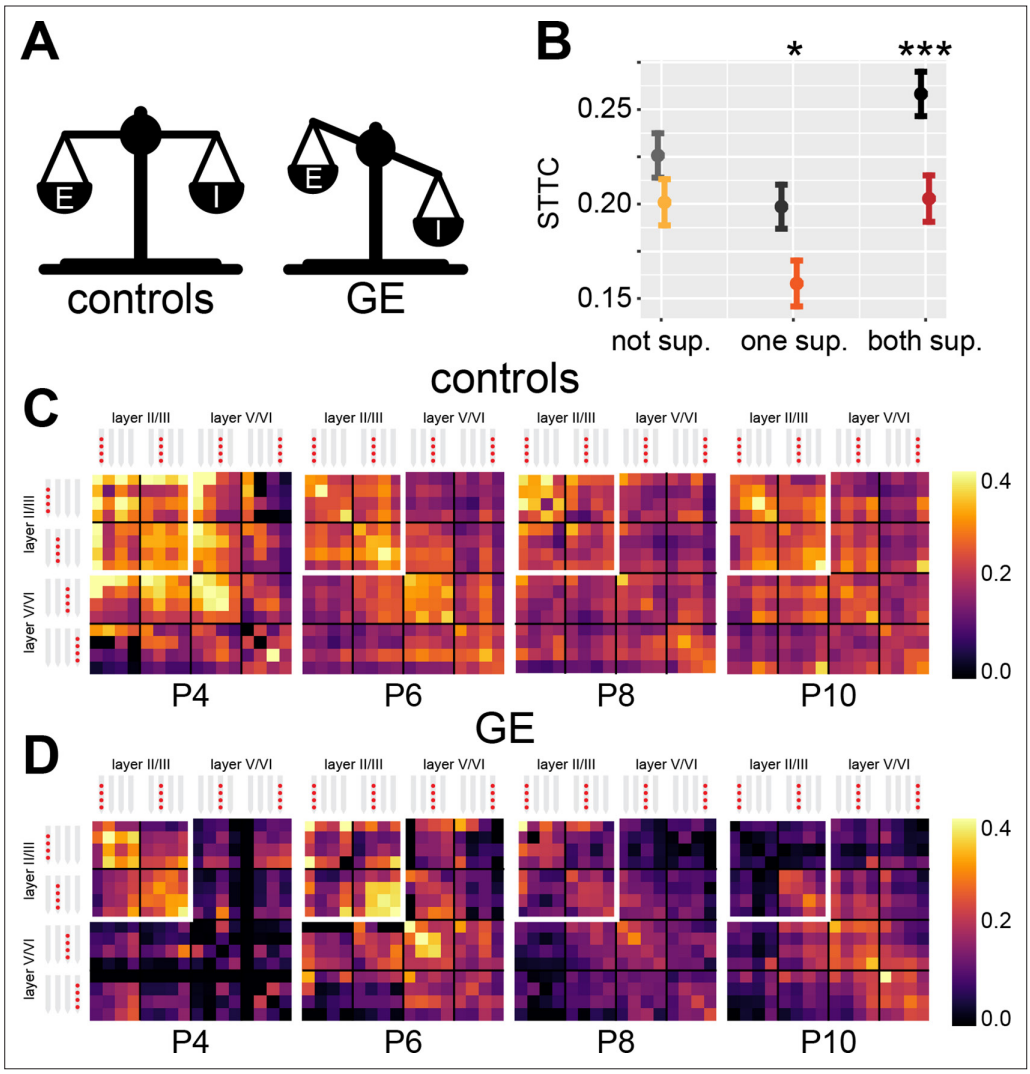

Figure 7. Genetic-environmental (GE) mice have reduced spike time tiling coefficient (STTC) values with specific spatial profiles. (**A**) Schematic representation of the excitation-inhibition (E-I) ratio imbalance affecting GE mice. (**B**) STTC of control and GE mice (n=18,839 and 11,051 spike train pairs; 33 and 30 mice, respectively) with respect to the number of neurons in the superficial layers in the medial prefrontal cortex (mPFC). (**C**) Weighted adjacency matrices displaying average STTC at 1 s lag of P4, P6, P8, P10, and control mice as a function of the recording sites in which the spike train pair has been recorded (n=18,839 spike train pairs and 33 mice). White inset indicates STTC values between spike trains that are located in the superficial layers of the mPFC. Color codes for STTC value. (**D**) Same as (**C**) for GE mice (n=11,051 spike train pairs and 30 mice).

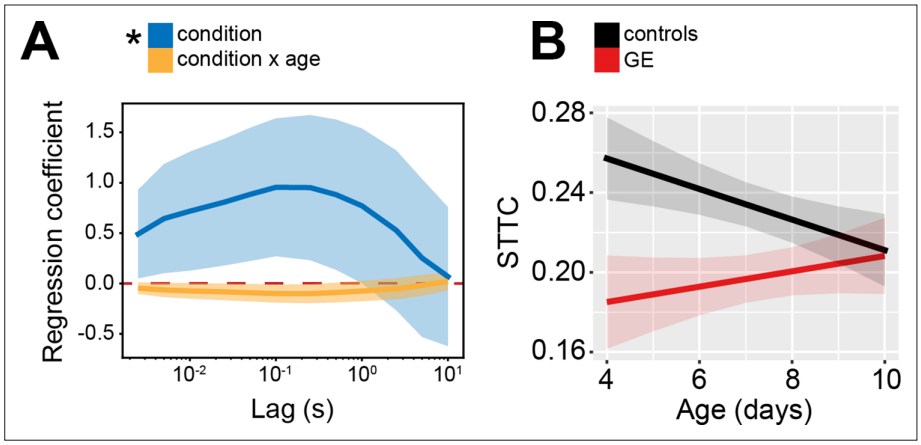

Figure 7—figure supplement 1. Age and spatial profile of spike time tiling coefficient (STTC) values in genetic-environmental (GE) and ES mice. (**A**) Multivariate linear regression coefficients as a function of STTC lag (*n*=29,890 spike train pairs and 63 mice). (**B**) STTC of control and GE mice (*n*=18,839 and 11,051 spike train pairs; 33 and 30 mice, respectively) over age. Asterisks in (**A**) indicate significant regression coefficients of the respective variable for STTC at 1 s lag. *p<0.05. In (**A**) regression coefficients are presented as mean and 95% CI. In (**B**) data are presented as mean ± SEM. Linear mixed-effect models. For detailed statistical results, see ***Supplementary file 1***.

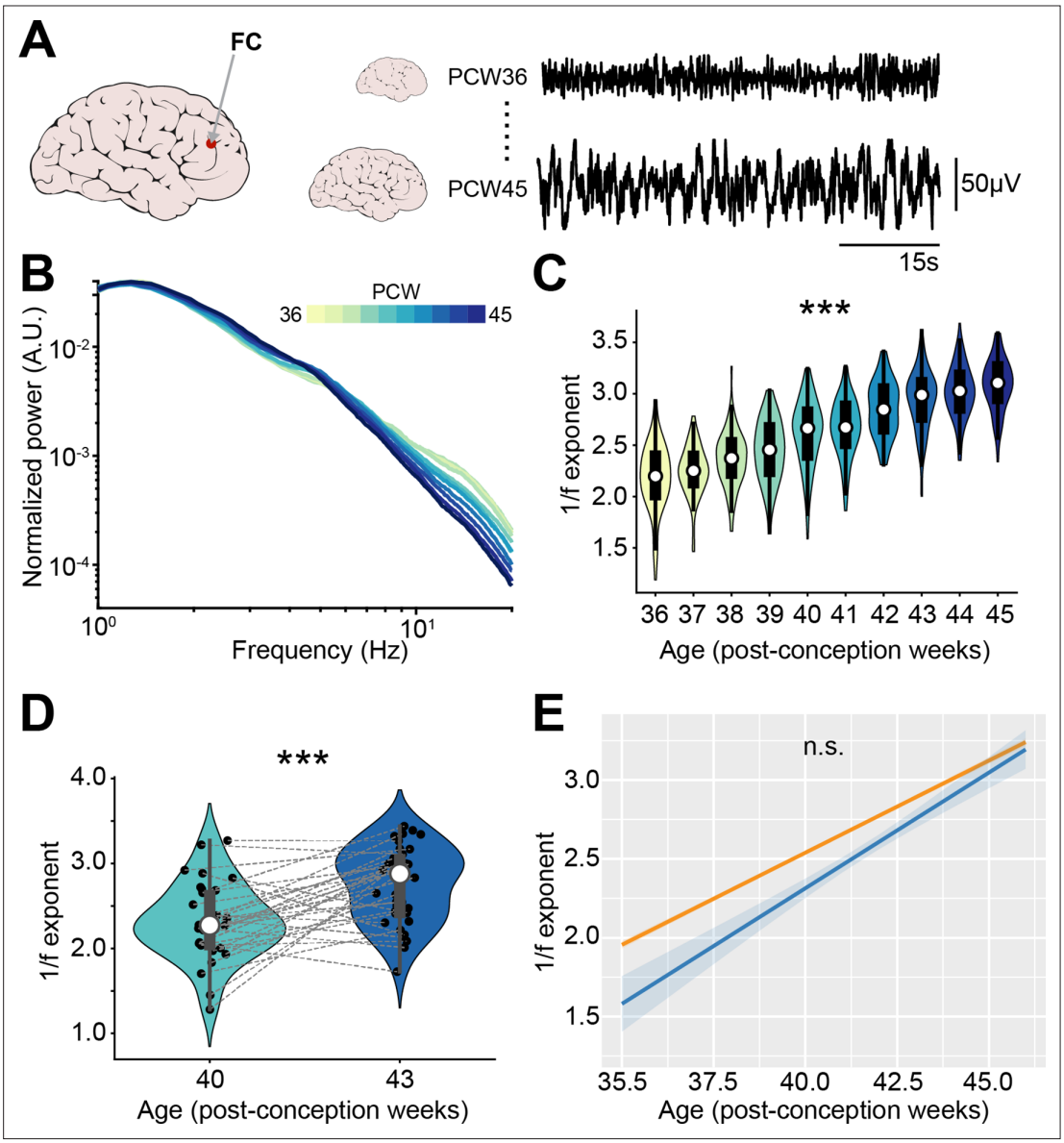

Figure 8. 1/f exponent of EEG recordings increases with age in newborn babies. (**A**) Schematic representation of EEG recording from frontal derivations of 36-45 post-conception week (PCW) newborn babies (left) displayed together with representative EEG traces from 36 and 45 PCW newborn babies (right). (**B**) Log-log plot displaying the normalized mean power spectral density (PSD) power in the 1–20 Hz frequency range of 36-45 PCW newborn babies (*n*=1110 babies). Color codes for age. (**C**) Violin plots displaying the 1/f exponent of 36-45 PCW newborn babies (*n*=1110 babies). (**D**) Same as (**C**) for 40 and 43 PCW newborn babies (*n*=72 EEG recordings and 40 babies). (**E**) 1/f exponent over age for the two EEG datasets (*n*=1110 babies and *n*=72 EEG recordings and 40 babies, respectively). In (**D**) black dots indicate individual data points. In (**C**) and (**D**) data are presented as median, 25th, 75th percentile, and interquartile range. In (**C**) and (**D**) the shaded area represents the probability distribution density of the variable. In (**B**) and (**E**) data are presented as mean ± SEM. Asterisks in (**C**) and (**D**) indicate significant effect of age. ***p<0.001. Linear model (**C**) and linear mixed-effect models (**D–E**). For detailed statistical results, see ***Supplementary file 1***.

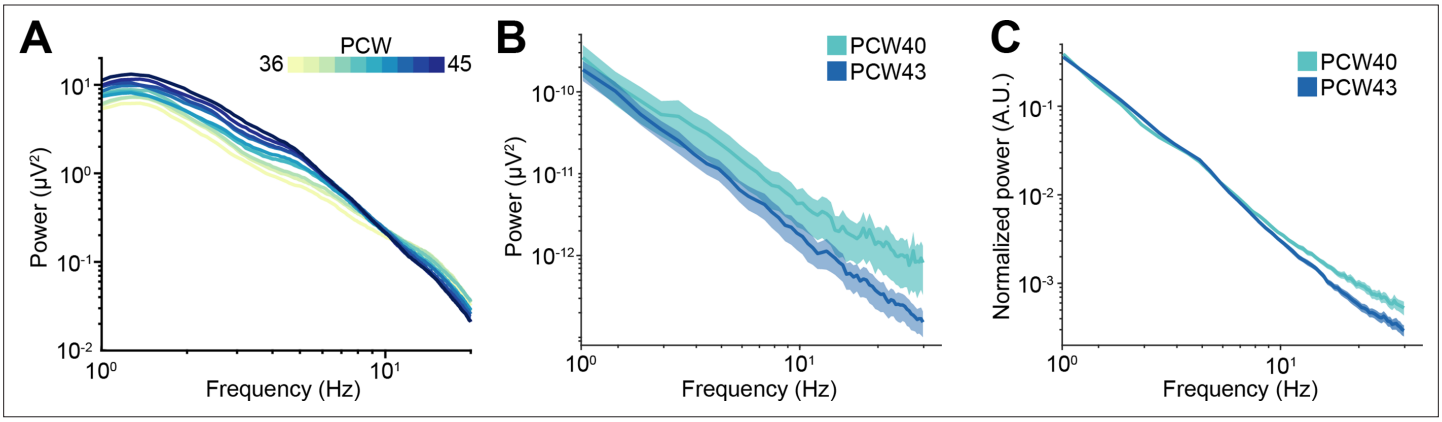

Figure 8—figure supplement 1. EEG power spectral densities (PSDs) of newborn babies. (**A**) Log-log plot displaying the mean PSD power in the 1–20 Hz frequency range of 36-45 post-conception week (PCW) newborn babies (*n*=1110 babies). Color codes for age. (**B**) Same as (**A**) for 40 and 43 PCW newborn babies (*n*=72 EEG recordings and 40 babies). Color codes for age. (**C**) Same as (**B**) for normalized mean PSD power. In (**A–C**) data are presented as mean ± SEM.